Discovery and characterization of SY-1365, a selective, covalent inhibitor of CDK7

Shanhu Hu[1], Jason J. Marineau[1], Nisha Rajagopal[1], Kristin B. Hamman[1], Yoon Jong Choi[1], Darby R. Schmidt[1], Nan Ke[1], Liv Johannessen[1], Michael J. Bradley[1], David A. Orlando[1], Sydney R. Alnemy[1], Yixuan Ren[1], Stephane Ciblat[2], Dana K. Winter[2], Anzhelika Kabro[2], Kevin T. Sprott[1], J. Graeme Hodgson[1], Christian C. Fritz[1], John P. Carulli[1], Emmanuelle di Tomaso[1] and Eric R. Olson[1]

[1]Syros Pharmaceuticals, Inc. 620 Memorial Dr, Cambridge, MA 02139, USA

[2]Paraza Pharma, Inc.7171 rue Frederick-Banting, Saint-laurent, QC, H4S 1Z9 Canada

Runny title: Discovery and characterization of a CDK7 inhibitor SY-1365

Keywords: CDK7 inhibitor, SY-1365, acute myeloid leukemia (AML), ovarian cancer,

Financial support: This study is supported by Syros Pharmaceuticals, Inc.

Correspondence author:

Shanhu Hu Ph.D.,

Syros Pharmaceuticals,

620 Memorial Drive, Cambridge MA 02139;

Phone: 617-674-9068

Email: shu@syros.com

Conflict of interest: SH, JJM, NR, KBH, YC, DS, NK, LJ, MB, DAO, SRA, YR, KS, JGH, CF, JPC, EdT and ERO have or had an equity position in Syros Pharmaceuticals, Inc.

Word count: 5000

Total of seven figures and tables.

Abstract

Recent studies suggest that targeting transcriptional machinery can lead to potent and selective anti-cancer effects in cancers dependent on high and constant expression of certain transcription factors for growth and survival. CDK7 is the catalytic subunit of the CDK-activating kinase (CAK) complex. Its function is required for both cell cycle regulation and transcriptional control of gene expression. CDK7 has recently emerged as an attractive cancer target since its inhibition leads to decreased transcript levels of oncogenic transcription factors, especially those associated with super-enhancers (SE). Here we describe a selective CDK7 inhibitor SY-1365, which is currently in clinical trials in populations of ovarian and breast cancer patients (NCT03134638). In vitro, SY-1365 inhibited cell growth of many different cancer types at nanomolar concentrations. SY-1365 treatment decreased MCL1 protein levels, and cancer cells with low BCL-XL expression were found to be more sensitive to SY-1365. Transcriptional changes in acute myeloid leukemia (AML) cell lines were distinct from those following treatment with other transcriptional inhibitors. SY-1365 demonstrated substantial anti-tumor effects in multiple AML xenograft models as a single agent; SY-1365-induced growth inhibition was enhanced in combination with the BCL2 inhibitor venetoclax. Anti-tumor activity was also observed in xenograft models of ovarian cancer, suggesting the potential for exploring SY-1365 in the clinic in both hematological and solid tumors. Our findings support targeting CDK7 as a new approach for treating transcriptionally addicted cancers.

Significance

Findings demonstrate the molecular mechanism of action and potent anti-tumor activity of SY-1365, the first selective CDK7 inhibitor to enter clinical investigation.

Introduction

The role of cyclin-dependent kinase 7 (CDK7) in regulating cell cycle progression and transcription has been described in both yeast (Kin28) and human cells(1-3). In cell cycle regulation, CDK7 complexes with CyclinH and Mat1 to form the CDK-activating kinase, (CAK), and phosphorylates CDK1,2,4 and 6 to promote cell cycle progression(2,3). As part of the multi-subunit transcription factor II human (TFIIH), CDK7 phosphorylates the C-terminal domain (CTD) of the RNA polymerase II (RNAPII) subunit Rbp1, with preference for the Ser5 and Ser7 residues of the YSPTSPS heptapeptide repeat. This CTD phosphorylation plays a regulating role in the ability of RNAPII to initiate a productive transcription cycle(1,4-6). Moreover, CDK7 activates CDK9 via T-loop phosphorylation, providing another layer of regulation on transcription initiation and elongation(7,8). Roles in DNA repair, transcription termination, RNA capping, and chromatin modification have also been described(1,9-11).

Based on findings in nonclinical models, CDK7 inhibition has emerged as a therapeutic approach in cancer. Though the downstream events of CDK7 inhibition have not been fully elucidated, decreased expression of oncogenes, including aberrantly expressed transcription factors associated with super-enhancers (SEs), has been described(12). Treatment with the small molecule CDK7 inhibitor THZ1 resulted in apoptosis and inhibition of tumor growth in several human tumor murine xenograft models, including T cell acute lymphoblastic leukemia (T-ALL)(13), high-grade glioma(14), melanoma(15), neuroblastoma(12), medullary thyroid carcinoma(16) hepatocellular carcinoma(17,18), esophageal squamous cell carcinoma(19), nasopharyngeal carcinoma(20), small cell

lung cancer (SCLC)(21), triple-negative breast cancer (TNBC)(22) and ovarian cancer(23). Notably, these animal models had minimal weight loss, suggesting the potential for a therapeutic margin based on enhanced sensitivity of tumor cells. Furthermore, THZ1 is reported to suppress adaptive resistance development towards several targeted cancer therapies(24).

Transcriptionally, THZ1 treatment recapitulated the effects of selective inhibition of an analogue-sensitive CDK7 variant with a bulky ATP analog that does not inhibit wild-type CDK7. Both pharmacological agents affected RNAPII pausing and the expression of a common set of genes(1,9).

Given that THZ1 lacked several features desired in a clinically applicable molecule, we executed medicinal chemistry on the THZ1 scaffold to identify a CDK7 inhibitor suitable for clinical investigation. We describe a new molecule, SY-1365, as more potent, selective, and metabolically stable than THZ1. SY-1365 is in clinical development as a single agent and in combination with standard of care agents in multiple ovarian and breast cancer populations (NCT03134638).

Materials and Methods:

Chemicals:

JQ1 (S7110), flavopiridol (S2679) and venetoclax (S8048) were purchased from Selleck Chemicals, LLC. NVP2 (HY-12214A) was purchased from MedChemExpress, LLC.

Detailed synthetic protocols for SY-314, SY-351, SY-1365, biotinylated SY-1365 and SY-1365 covalent docking to CDK7 can be found in Supplementary Materials and Methods.

Kinase Activity Assay:

Compound potencies were determined for each CDK by measuring loss of activity of the kinase on a peptide substrate. All assays included active CDK protein purified with Cyclin protein (CyclinH and Mat1 with CDK7), ATP, substrate peptide (5-FAM-YSPTSPSYSPTSPSYSPTSPSKKKK with CDK7), and compound or DMSO. After incubation, the amount of phosphorylated peptide product was measured using Caliper/LabChip EZ Reader. Percent inhibition by the compound was determined by comparing the amount of substrate converted to product with compound versus DMSO control. Further details can be found in Supplementary Materials and Methods.

Determination of K_I and k_{inact}:

The CDK7 inhibition kinase assay was performed as above, however compound and CDK7/CyclinH/MAT1 complex were pre-incubated for 0, 5, 10, 20, 30, 60min prior to reaction initiation with ATP and substrate. CDK7/CyclinH/MAT1 concentration was increased to 30nM, with a 5min reaction time. The time-dependent decay of enzyme activity due to covalent inhibition was used to fit the k_{inact} and K_I values for each compound(25).

Pharmacokinetics:

Animals were dosed intravenously according to their bodyweight (5ml/kg). Blood was collected at 0.25,0.5,1,2,4,6,10 and 24h post-administration and centrifuged to obtain plasma. Plasma was processed for bioanalysis using LC-MS/MS analysis (Waters Aquity UPLC and API 5500 or API 4000 triple quad mass spectrometer).

Antibodies:

The information for antibodies used in this study can be found in Supplementary Table S1.

Cell lines:

HL60 (ATCC® CCL-240), RPE-hTERT (ATCC® CRL-4000), BJ-hTERT (ATCC® CRL-4001), THP1 (ATCC® TIB-212), HCC70 (ATCC® CRL-2315), KG-1 (ATCC® CCL-246), Kasumi-1 (ATCC® CRL-2724) and MDA-MB-468 (ATCC® HTB-132) were purchased from ATCC. ML-2 (ACC-15) was purchased from DSMZ. All cell lines were cultured according to vendor's instruction at 37°C in 5% CO_2 in a humidified incubator. All cell lines used in the study were under passage 15. Mycoplasma test was not performed.

Antiproliferation assay:

Three hundred and eighty-six cell lines were treated with SY-1365 at following concentrations(μM): 0.0005, 0.0015, 0.0046, 0.014, 0.041, 0.12, 0.37, 1.1. Cells were incubated with compound for 72h or at least two doubling times if they were slow growing. CellTiter Glo (G7570, Promega) signal was measured before treatment on day0 and then a minimum of 3 or maximum of 6 days after treatment depending on the cell line.

Simultaneously the signal was measured from the cell line treated with DMSO for the same duration.

The CellTiter Glo signals after treatment with drug at increasing concentrations were normalized to DMSO to obtain the relative cell count. A dose response curve was fit to these relative counts using the GRcalculate and GRlogisticFit functions from the R package GRmetrics(26). Response metrics calculated from the cell line data are in Supplementary Table S2 and described in Supplementary Materials and Methods. Based on these response metrics, we developed an algorithm for classifying cell lines into two categories, “low-sensitive/insensitive” or “high-sensitive” to SY-1365 (Supplementary Table S2, Supplementary Materials and Methods).

Apoptosis assay:

For TNBC and immortalized normal cell lines, logarithmically growing cells were seeded the day before treatment and grown to 60-80% confluence. For AML cell lines, cells were seeded at 0.5 million per milliliter and dosed 2h later. For all cell lines, cells were dosed with either DMSO or the indicated dosages of SY-1365 for 48h before staining with AnnexinV and propidium iodide (10010-02, Southernbiotech, ApoScreen™ AnnexinV Apoptosis Kit) following vendor’s recommendations. Samples were analyzed by flow cytometry and results were analyzed on FlowJo V10.

Occupancy assay:

To determine the ratio of SY-1365-occupied- to unoccupied-CDK7 in each cell line, cells were treated with DMSO or SY-1365 for the indicated time before protein samples were harvested in MPER mammalian protein extraction reagent (78501, ThermoFisher) with 1X Halt™ Protease and Phosphatase Inhibitor Cocktail (100X) (78440, Life technologies) and 1X Benzonase® Nuclease (1000X) (E1014-25KU, sigma-aldrich). Unoccupied-CDK7 in the lysates was precipitated by incubating with biotinylated SY-1365 overnight at 4°C. For the immunoblotting readout, Dynabeads® MyOne™ Streptavidin T1 beads (65602, Thermofisher) were used to precipitate biotinylated SY-1365 captured CDK7. For the Meso Scale Diagnostics (MSD) readout, MSD bare plate (L15XA-3, Meso Scale Diagnostics, Rockville, MD) and MSD streptavidin plates (L15SA-5, Meso Scale Diagnostics, Rockville, MD) were used to capture input and free CDK7, respectively, following vendor's protocol. Schematic overview of the assays is shown in Supplementary Fig.S1.

To determine percent occupancy in tumor lysate samples, the following equation was used: $\%CDK7_{occ}$=(1-free-CDK7/free-CDK7 of vehicle treated sample)*100%. This calculation assumes the occupancy in vehicle treated tumors to be 0%.

Immunoblotting:

Cells were harvested at indicated time points as in occupancy assay. Target protein level was evaluated via immunoblotting as previously described(27).

Microarray Analysis:

THP1 cells were treated with 100nM SY-1365, 25nM NVP2, 200nM flavopiridol, 250nM JQ1 or vehicle control for 2 or 6h before total RNA harvest using mirVana miRNA isolation kit (AM1560, Thermofisher). Experiments were done in triplicate. ERCC spike-in mix (4456740, Thermofisher) was added to each sample for normalization according to vendor's instruction. 1000ng of RNA from each sample was profiled on Affymetrix PrimeView microarrays using manufacturer's instructions. Data normalization and processing are described in Supplementary Materials and Methods. Normalized expression values per probe are shown in Supplementary Table S3. Expression data were submitted to GEO (accession GSE121431).

H3K27ac ChIP-seq

ChIP-seq with H3K27ac antibodies was performed in THP1 cells and SEs were called as described previously(28,29). SE associated genes were defined as those whose promoters overlapped a SE.

Analysis of RNA-seq data from HCT116 CDK7 analogue-sensitive cells:

RNA-seq data for wildtype and CDK7 analog-sensitive HCT116 cells(1) was obtained from the GEO expression database (GSE100040). Raw RNA-seq reads were aligned to the human hg19 build and expression levels per gene in the Ensembl database(30) were quantified using RSEM(31). Differential gene expression between the wildtype and $CDK7^{AS}$ conditions were determined using DESEQ2(32). Log-fold values computed by DESEQ2 were used as input to the GSEA algorithm (below).

Gene Set Enrichment Analysis:

Gene set enrichment analysis was performed on gene-sets from the REACTOME database(33), obtained using the Graphite package(34). Enrichment analysis was performed using the GSEA algorithm previously described(35) with modifications as described in the Supplementary Materials and Methods.

In vitro Synergy:

Logarithmically growing cells were seeded in 384-well plates (Thermo) at 1,500 cells/well 1h before compound treatment with HP D300e Digital Dispenser. Compound distribution is shown in Supplementary Fig.S2. Concentrations were selected to cover the full isobologram of activity based on the activity of single agents. Cell plates were incubated for 3 days in a 37°C incubator before viability evaluation using ATPlite (6016949, Perkin Elmer) following manufacturer protocols. Data was analyzed in CalcuSyn utilizing the median effect principle of Chou-Talalay(36).

Mouse xenograft study:

Six-to-eight-week-old female mice were implanted subcutaneously with Kasumi-1, ML-2, KG-1, OVCAR3 cells or OV15398 specimen (Crownbio Biosciences). All studies were conducted following an approved IACUC protocol. NOD-SCID mice were used for Kasumi-1, ML-2 and OV15398 models, CB17-SCID mice were used for KG-1 model and BALB/c nude mice were used for OVCAR3 model. After tumor cell inoculation, tumor volumes were measured twice weekly using a caliper. Once tumors had reached 150-200mm^3, mice were randomized into groups for dosing. Group dosing details are shown

in Supplementary Table S4. Animal body weight was measured twice weekly. Tumor growth inhibition (TGI) was calculated as follows: TGI(%)=(1-($TV_{Treatment/Dx}$-$TV_{Treatment/D1}$)/($TV_{Control/Dx}$– $TV_{Control/D1}$))×100%.

Results

Discovery of SY-1365

The previously described CDK7 inhibitor THZ1 demonstrated the feasibility of a small molecule irreversibly inhibiting CDK7 through covalent attachment to a cysteine residue (Cys312) located outside the ATP binding pocket(37). A medicinal chemistry effort based on THZ1 was undertaken to improve potency, selectivity and metabolic stability to identify molecules suitable for clinical development (Fig.1A). Optimization of k_{inact} (the maximal covalent deactivation rate constant) and K_I (the apparent covalent inhibitor affinity for a target enzyme)(25) were important parameters in the evolution of the series. Efforts to improve the potency, selectivity and stability of THZ1 included saturation of the central ring. Indeed, it was found that 1*S*,3*R*-cyclohexanediamine in the intermediate SY-314 provided a 2.4-fold decrease in K_I and increased selectivity over CDK2 and CDK12. This substitution also served to reduce the *in vivo* clearance by 7.6-fold to 17ml/min/kg (Fig.1A). However, the efficiency of covalent enzyme inhibition, as measured by k_{inact}/K_I, was still lower than desired at 0.013$\mu M^{-1}s^{-1}$. To overcome this limitation, the effects of altering the electronic characteristics of the aromatic ring attached to the covalent warhead were investigated. Replacing the benzamide linker with an optimal electron-withdrawing picolinamide to generate SY-351 resulted in an increase of k_{inact} to 11.3h^{-1} and an overall improvement of k_{inact}/K_I to 0.050$\mu M^{-1}s^{-1}$(Fig.1A). This provided 12-fold more

potent cellular target engagement compared to SY-314 at the cost of increased clearance. Further elaboration of the chiral cyclohexanediamine ring with a methyl group increased hinderance around the amide linker and restricted the accessible conformations of the warhead. SY-1365 exhibited additional improvements in K_I and selectivity with a somewhat reduced k_{inact} resulting in the highest k_{inact}/K_I in the series, 0.131$\mu M^{-1}s^{-1}$, a value comparable with marketed covalent kinase inhibitors(37). SY-1365 also exhibited the lowest plasma clearance in the series at 5.6ml/min/kg in mouse (Fig.1A).

Docking of SY-1365 with a model CDK7 structure (Fig.1B) highlights the preservation of key interactions of the indole and chloropyrimidine rings present in THZ1(37), including the hinge binding of the aminopyrimidine with Met94 and contact between the chlorine atom and the phenylalanine gatekeeper (Phe91). Improved shape complementarity and hydrophobic interactions from the chiral cyclohexane-1,3-diamine core are highlighted by close contact with the solvent accessible surface of the protein in this region and likely contribute to the increased potency and selectivity of this series relative to THZ1. The optimized linker provides an appropriate vector to covalently engage Cys312.

Covalent attachment of SY-1365 to CDK7 *in vitro* was shown by a time-dependent shift in IC_{50} following 5-60min preincubation of compound and enzyme (Supplementary Fig.S3A). An increase in IC_{50} with 2mM ATP compared with ATP at apparent K_M demonstrates ATP-competitive inhibition (Supplementary Fig.S3B).

Biochemical selectivity of SY-1365 was evaluated in a panel of closely related CDKs and in a broader kinase panel (Fig.1C and Supplementary Table S5). The SY-1365 IC_{50} for CDK7 at 2mM ATP without compound preincubation was 369nM whereas with all other CDKs including CDK2,9 and 12, SY-1365 had an IC_{50} of 2μM or greater. In the kinome screen (DiscoverX KINOMEscan) (Supplementary Table S6) 8 out of 468 kinases including CDK7 were inhibited greater than 90% by SY-1365 at 1μM. Though biochemical selectivity is useful for comparing compounds and to identify signals of potential pharmacological significance it does not reflect the selectivity that may occur *in vivo* due to the covalent mode of inhibition. Occupancy of CDK7, but not kinases lacking an appropriately positioned cysteine residue, is anticipated to persist following clearance of the compound from systemic circulation(38).

Target engagement and CDK7-dependent phosphorylation inhibition in cells

To test the concentration dependence of target engagement by THZ1, SY-314, SY-351 and SY-1365 in living cells, HL60 cells were treated with increasing concentrations of each compound for 1h and the CDK7 occupancy was quantified by both immunoblotting and MSD (Supplementary Fig.S1). Dose-dependent target engagement is observed after 1h of treatment in all compounds, with lower EC_{50} observed in SY-1365 and SY-351 compared to THZ1 and SY-314 (Fig.2A,B, Supplementary Table S7, S8A).

The impact of SY-1365 treatment on phosphorylation of several CDK7 substrates including Thr160 of CDK2 and Ser2,5 and 7 residues of the RNAPII CTD was evaluated in THP1, HCC70 and RPE-hTERT cell lines (Fig.2C, Supplementary Table S8B). CDK7

was fully occupied by SY-1365 in all three cell lines (Fig.2C,Supplementary Fig.S4,Table S8B,S9). RNAPII CTD phosphorylation at Ser2,5 and 7 sites was inhibited by SY-1365 in a dose and time dependent manner in all cell lines, supporting CDK7's role in transcriptional control(4). In addition, CDK2 phosphorylation at Thr160 was inhibited by SY-1365 treatment in a dose and time dependent manner (Fig.2C,Supplementary Fig.S4,Table S8B,S9). Massive cell death was observed in samples treated with 100 and 250nM SY-1365 at 24 and 48h, resulting in loss of total CDK7, CDK2, RNAPII and tubulin.

Anti-tumor effect of SY-1365 in vitro

The antiproliferative effect of SY-1365 was tested in 386 human cell lines representing 26 cancer types. Multiple cell lines from various cancer types showed significant growth-inhibition and cell-killing by SY-1365 in nanomolar range, with leukemia cell lines among the most sensitive (Fig.3A,B,C). The concentration of SY-1365 at which growth is reduced by half (IC_{50}) or cell killing begins (GR_0) only spans about a log-fold difference in concentrations for the majority of cell lines within indications (Fig.3A,C). However, the distribution of GR_{max} suggests that cell lines can vary greatly in their degree of cytotoxicity ranging from cytostatic (GR_{max}~0) to highly cytotoxic (GR_{max}=-1) (Fig.3B). All indications examined have at least some cell lines showing a cytotoxic response to SY-1365, although the proportion of these cytotoxic responders varies across indications (Fig.3B).

To examine the mechanism by which SY-1365 causes cell death, the ability of SY-1365 to induce apoptosis was evaluated in several cell lines. Following incubation with SY-1365 the percentage of apoptotic cells was quantified by flow cytometry following

annexinV and propidium iodide (PI) staining. Apoptosis was observed in cancer cell lines (THP1, ML2, HCC70, MDA-MB-468), but not in hTERT-immortalized cell lines (RPE-hTERT, BJ-hTERT) (Fig.4A). Consistent with induction of apoptosis, PARP cleavage was observed in SY-1365 treated THP1 and HCC70 cells as early as 6h following treatment at 100nM, but not in RPE-hTERT treated up to 48h at 250nM (Fig.4B).

Since the 386-cell-line panel showed variation in apoptotic response and a wide range for the response metrics GR_{max} (the magnitude of cell-killing) and GR_0 (the lowest concentration inducing cell death) (Supplementary Table S2), we developed an algorithm that classified cell lines and identified biomarkers of “high-sensitive” and “low-sensitive” cell lines based on the SY-1365 growth-response curves (Fig.5A, Supplementary Materials and Methods). This algorithm takes into account both GR_{max} and GR_0. Classifying cell-lines in this way ensured that a cell line classified as “high-sensitive” was growth-inhibited at low concentrations and that the inhibition by SY-1365 resulted in cell death. Using this algorithm, we classified 267 and 119 cell lines as “high-sensitive” and “low-sensitive” respectively. (Fig.5A and Supplementary Table S2).

To identify genes whose baseline expression level in a cell line was predictive of membership in either the “high-sensitive” or “low-sensitive” response classes, we performed a genome-wide analysis using microarray and RNA-Seq expression data from CCLE(39) for cell lines in common with our cell line panel. Among 386 cell lines screened in our study, 303 had matched microarray datasets and 294 had matched RNA-seq datasets (Supplementary Materials and Methods). Strikingly, expression of the anti-

apoptotic gene BCL-XL (also known as BCL2L1) was the most strongly associated with response to SY-1365 across all cell lines agnostic to indication (Balanced accuracy=70%,74%, empirical *p*-value=0.01,0.002, for microarray and RNA-seq respectively) (Fig.5B). This association of BCL-XL expression and response to SY-1365 was consistent across multiple tumor types, and therefore was not driven by differential sensitivities across indications (Supplementary Fig.S5). The association of low BCL-XL expression with high SY-1365 response is consistent with the induction of apoptosis by SY-1365.

Based on the results of the gene-expression analysis, we hypothesized that cell lines with low level of BCL-XL are more sensitive towards SY-1365 due to downregulation of anti-apoptotic proteins, making cells more prone to apoptosis. Examination of the anti-apoptotic protein MCL1 by immunoblotting indeed showed a consistent dose- and time-dependent decrease after SY-1365 treatment in multiple cell lines (Fig.5C, Supplementary Table S10).

If SY-1365-induced reduction of MCL1 contributes to cytotoxic responses of BCL-XL low cell lines, then BCL-XL-low cell lines should also be sensitive to loss of MCL1 by CRISPR. Thus, we compared the MCL1 essentiality scores from the public genome-wide CRISPR screen, Avana(40), to expression of all genes available from CCLE across 339 cell lines tested in common. We predicted that BCL-XL expression would be negatively correlated with MCL1 essentiality. Supporting our hypothesis, we found that BCL-XL expression had the strongest correlation (negative or positive) with MCL1 essentiality across all genes

(cor=-0.42, pvalue=1.3X10^-15) (Supplementary Fig.S6A,B). Interestingly, no correlation of MCL1 essentiality was observed with expression of MCL1 itself (Supplementary Fig.S6A,C, cor=0.035, pvalue=0.52). Finally, we directly compared the sensitivity of cell lines to SY-1365 to the essentiality of all genes for cell lines in common to both screens. We found that MCL1 was the top gene whose essentiality was most strongly associated with SY-1365 sensitivity (Fig.5D).

Together, these data suggest that low levels of BCL-XL are associated with greater dependence on MCL1 protein. Therefore, the reduction of MCL1 protein by SY-1365 may be a significant contributor to the sensitivity of low BCL-XL cells to SY-1365-induced apoptosis.

Transcriptional changes induced by SY-1365

To test the hypothesis that SY-1365 treatment results in gene expression changes reflective of CDK7's role in transcription, we performed genome-wide expression profiling in the AML cell line THP1 following SY-1365 exposure for 2 or 6h. Additionally, we compared the effects to those resulting from treatment with other small molecules that target transcription components: CDK9 (NVP2), BRD4 (JQ1), and multiple CDKs (flavopiridol) (Supplementary Table S3). The dose selected for each compound is its antiproliferative EC_{90} in THP1.

Principal component analysis of the expression data identified 5 distinct clusters of transcriptional profiles (Fig.6A). Clusters 1 and 2 contain all the untreated samples as well

as all treated samples measured at the shorter 2h timepoint, suggesting these clusters represent a relatively unperturbed profile. At the 6h time point clear differences in the transcriptional profiles are apparent. Cluster 4 is comprised solely of samples treated with SY-1365 for 6h indicating that a unique transcriptional response was elicited by SY-1365 compared to the other inhibitors. Differential gene expression analysis (Supplementary Materials and Methods) found broad downregulation of transcription with all three CDK inhibitors (SY-1365, NVP2 and flavopiridol) (Supplementary Table S11). However, compared with NVP2 and flavopiridol treatment, a much smaller set of genes was downregulated by SY-1365, consistent with higher CDK specificity relative to flavopiridol, and suggesting that CDK7 inhibition may have a more targeted impact on a specific set of genes than CDK9 inhibition (Supplementary Table S11). Moreover, consistent with previous studies(12,13,22,23,41), SY-1365 preferentially downregulated super-enhancer-tagged oncogenic transcription factor genes compared to housekeeping genes (Fig.6B). Compared to genes with similar basal expression profiles, super-enhancer associated genes were found to be significantly enriched for downregulation by SY-1365 (unweighted GSEA p-value=6X10^-5, Supplementary Fig.S7). While flavopiridol and NVP2 treatments did not show any such preferential enrichment (flavopiridol p-value 0.59, NVP2 p-value 0.84), JQ1 showed even greater specificity for super-enhancer associated genes (JQ1 p-value<10^-324).

To evaluate whether any specific biological pathways were preferentially downregulated upon SY-1365 treatment, we performed a Gene Set Enrichment Analysis (GSEA)(35) (Methods, Supplementary Materials and Methods). We evaluated the enrichment of gene

expression changes in 1208 pathways from the REACTOME database(33). 25 out of 1208 pathways had a significant enrichment for genes with expression changes after SY-1365 treatment (p-value<0.001, Supplementary Table S12). Among these pathways, the most significantly enriched were cell cycle related pathways and DNA damage repair related pathways, especially those related to homologous recombination repair (Fig.6C,D). To elucidate which pathway effects were most likely due to inhibition of CDK7, we performed a similar analysis using the reported gene expression changes due to inhibition of CDK7 in an analog-sensitive model(1). We observed that while a larger number of pathways were downregulated in the $CDK7^{AS}$ system compared to SY-1365 treatment (p-value<0.001; 92/1208 for $CDK7^{AS}$ versus 25/1208 by SY-1365), cell cycle and homologous recombination related DNA repair pathways were the most significantly downregulated pathways in both systems (Fig.6C,D).

As inhibition of DNA repair is an active area of development for cancer therapies, we sought to understand which pathways of DNA repair were specifically affected by SY-1365, and if that could be attributed to CDK7i. We evaluated four distinct pathways related to different aspects of DNA damage: homologous recombination, mismatch repair, nucleotide excision repair and non-homologous end joining. In addition to homologous recombination DNA damage repair, we found that mismatch repair was significantly downregulated (Supplementary Table S13) but nucleotide excision repair and non-homologous end-joining were not, and that impact was specific to treatments targeting CDK7.

SY-1365 tumor growth inhibition in xenograft models

Since SY-1365 treatment did not induce myelosuppression in mice (Supplementary Fig.S8), its potential tumor growth inhibition *in vivo* was evaluated in multiple xenograft models up to six weeks treatment. AML cell-line xenograft models Kasumi-1 and ML-2 were treated once or twice per week with SY-1365 at 40mg/kg. At the end of 4 weeks of treatment in the Kasumi-1 model, regression was observed in both the twice weekly and once weekly dosing arms with values of 116% and 108% tumor growth inhibition (TGI) respectively (Fig.7A, red and blue lines), and was sustained during 7-day post treatment observation. Treatment of Kasumi-1 tumors with SY-1365 at 20mg/kg twice weekly resulted in moderate anti-tumor activity with 62% TGI at the end of treatment and 37% seven days after the final dose (Fig.7A, grey line). Substantial TGI in the ML-2 AML xenograft model was also observed (Fig.7B). Anti-tumor activity was also observed in ovarian cancer xenograft models. SY-1365 (30mg/kg twice weekly) was active in both the ovarian cell line derived model (OVCAR3) and a patient derived model (OV15398) (Fig.7C and D).

SY-1365 is synergistic with venetoclax

The anti-apoptotic BCL2 inhibitor venetoclax is approved for the treatment of chronic lymphocytic leukemia (CLL) and small lymphocytic lymphoma (SLL) as single agent and in AML in combination with azacitidine, decitabine, or low-dose cytarabine(42). Given the induction of apoptosis in AML cell lines with SY-1365 (Fig.3,4) we investigated the combination of SY-1365 and venetoclax in four AML cell lines (Kasumi-1, ML-2, THP1 and KG-1). SY-1365 synergized with venetoclax in all cell lines as evidenced by most of

the data points below and left of the red line in the isobologram (Supplementary Fig.S9 red line represents expected data from an additive interaction).

We tested the combination of SY-1365 and venetoclax *in vivo* using the KG-1 xenograft model. As shown in Fig.7E, once weekly 40mg/kg SY-1365 and once daily 50mg/kg venetoclax as single agents showed moderate anti-tumor activity at the end of the study (TGI= 62.6% and 48.4%, respectively), while combination of the two at the same dosing regimen resulted in TGI of 87.5% at the end of the study.

Discussion

In this study we describe a potent and selective CDK7 inhibitor, SY-1365, that inhibits growth of tumor cells *in vitro* as well as in mouse tumor xenograft models. SY-1365 induced apoptosis in tumor cells, while in hTERT immortalized, non-cancerous cells minimal apoptosis was observed despite complete target occupancy. These, and published data in non-clinical models of a variety of tumor types, support the hypothesis that tumor cells have a dependency on CDK7 that is distinct from normal cells, providing a rationale for investigating CDK7 inhibitors in the clinic(12-15,17-23). SY-1365 was the first selective CDK7 inhibitor to enter clinical development and is currently being investigated as a single agent and in combination with standard of care agents in specific groups of ovarian and breast cancer patients (NCT03134638).

Development of SY-1365 was motivated by the discovery and characterization of a tool compound, THZ1, which provided validation that covalent CDK7 inhibition through a

cysteine residue at position 312 was a viable approach for inhibiting the growth of multiple tumor types in non-clinical models(12-16,18-23). Starting with the THZ1 scaffold, optimization of the three-dimensional shape and electron-withdrawing characteristics of the two rings linking the hinge binding element to the covalent warhead improved the binding potency (K_I) and the deactivation rate constant (k_{inact}). The resulting k_{inact}/K_I for SY-1365 affords substantially improved potency with rapid covalent CDK7 deactivation as compared to THZ1 (Fig.1A). This efficiency of covalent inhibition supports the ability of the molecule to engage the cysteine 312 residue in a cellular environment.

In addition to demonstrating direct engagement of CDK7, we showed that downstream phosphorylation targets of CDK7 are also affected upon SY-1365 treatment, including Ser2,5, and 7 in RNAPII CTD and Thr160 of CDK2. Interestingly, while direct target engagement and downstream phosphorylation of RNAPII CTD and CDK2 were similar in all cell lines, cancer cell lines were more susceptible to SY-1365 mediated apoptosis than the non-cancer lines. The difference in susceptibility in cancer vs noncancer cells appears to translate into the *in vivo* setting as we observed that SY-1365 inhibited tumor cell growth in murine xenograft models at exposures that led to minimal weight loss of the animals (Fig.7). To further investigate the potential therapeutic window, we demonstrated that SY-1365 did not have a major effect on blood cell counts following treatment of mice for 5 days, whereas the less selective CDK-inhibitor dinaciclib induced a substantial decrease in blood cells (Supplementary Fig.S8).

SY-1365 inhibits growth of a range of cell lines from multiple tumor types (Fig.3). Using publicly available genome-wide mRNA expression data for the treated cell lines we identified that cell lines with low expression of the anti-apoptotic gene BCL-XL are more sensitive to SY-1365-induced apoptosis than cell lines with high BCL-XL expression. Further, we found that SY-1365 down-regulates the MCL1 protein (Fig.5C), leading to a model in which CDK7 inhibition lowers MCL1 protein levels, leading to apoptosis in cells that are low in BCL-XL. Interestingly, we did not see consistent MCL1 down-regulation at the mRNA level at examined timepoints (Supplementary Table S3), only at the protein level. MCL1 is heavily regulated post-transcriptionally and can be phosphorylated by CDK1/2(43). It is possible that CDK7 inhibition decreases CDK1/2 function and leads to MCL1 protein degradation. More work is required to fully understand the relationship between CDK7, MCL1, and BCL-XL.

In addition to lowering MCL1 protein, SY-1365 treatment induces changes in cell cycle and DNA repair pathways that likely contributes to apoptosis of cancer cells. We compared gene expression changes induced in THP1 cells by SY-1365 to changes induced with pan-CDK (flavopiridol), CDK9 (NVP2) or BRD4 (JQ1) inhibitors. While SY-1365, NVP2 and flavopiridol all showed broad gene down regulation, the CDK7-specific SY-1365 impacted fewer genes and had a unique transcriptional profile.

Genes involved in cell cycle and two DNA repair pathways, homologous recombination repair and mismatch repair, are strongly and specifically down-regulated by SY-1365. This observation is consistent with previous literature investigating the effects of THZ1 in

ovarian cancer(23) and small cell lung cancer(21) and supported by our analysis of gene expression data from CDK7 analogue-sensitive cells(1). This finding is particularly interesting since CAK can function within TFIIH or on its own and may influence cell cycle and DNA repair through either or both. Further investigation is ongoing to understand the multiple ways by which SY-1365 inhibits cancer cell growth through affecting cell cycle, DNA repair, and apoptotic pathways.

Our results suggest that SY-1365 could have therapeutic value alone or in combination with approved therapies. SY-1365 monotherapy administered to multiple mouse xenograft models showed tumor growth inhibition and even tumor regression (Fig.7A-D). To test for combination effects, we combined SY-1365 with the BCL2 inhibitor, venetoclax which was recently approved for CLL, SLL and AML. We showed that combination of SY-1365 and venetoclax was synergistic in all three AML cell lines tested, and in a xenograft model the combination was more efficacious than either agent alone (Fig.7E). These findings provide rationale for investigating SY-1365 in combination with venetoclax in the clinic in AML.

Though the focus of the mechanistic work described here was in AML, the role of CDK7 in other tumor types and the activity of SY-1365, and the parent compound THZ1, in ovarian and breast cancer xenograft models suggests there is a broad opportunity to explore SY-1365 in multiple tumor types. To this end, SY-1365 was investigated clinically in a single agent dose-escalation study in solid tumors. The clinical trial is being expanded

to test SY-1365 monotherapy as well as combination treatments in particular types of ovarian and breast cancer (NCT03134638).

Acknowledgement

We thank Dr. Claudio Chuaqui for his help in reviewing the manuscript. We thank everyone at Syros Pharmaceuticals for their support. A granted U.S. patent pertaining to the results presented in this paper is USPN 10,059,690.

References:

1. Ebmeier CC, Erickson B, Allen BL, Allen MA, Kim H, Fong N, *et al.* Human TFIIH Kinase CDK7 Regulates Transcription-Associated Chromatin Modifications. *Cell Rep* **2017**;20:1173-86
2. Larochelle S, Merrick KA, Terret M-E, Wohlbold L, Barboza NM, Zhang C, *et al.* Requirements for CDK7 in the assembly of CDK1cyclinB and activation of CDK2 revealed by chemical genetics in human cells. *Mol Cell* **2007**;25:839-50
3. Schachter MM, Merrick KA, Larochelle S, Hirschi A, Zhang C, Shokat KM, *et al.* A Cdk7-Cdk4 T-loop phosphorylation cascade promotes G1 progression. *Mol Cell* **2013**;50:250-60
4. Jeronimo C, Collin P, Robert F. The RNA Polymerase II CTD: The Increasing Complexity of a Low-Complexity Protein Domain. *J Mol Biol* **2016**;428:2607-22
5. Chen F, Gao X, Shilatifard A. Stably paused genes revealed through inhibition of transcription initiation by the TFIIH inhibitor triptolide. *Genes Dev* **2015**;29:39-47
6. Serizawa H, Conaway JW, Conaway RC. Phosphorylation of Cterminal domain of RNA polymerase II is not required in basal transcription. *Nature* **1993**;363:371–4
7. Kwak H, Lis JT. Control of transcriptional elongation. *Annu Rev Genet* **2013**;47:483-508
8. Larochelle S, Amat R, Glover-Cutter K, Sanso M, Zhang C, Allen JJ, *et al.* Cyclin-dependent kinase control of the initiation-to-elongation switch of RNA polymerase II. *Nat Struct Mol Biol* **2012**;19:1108-15
9. Nilson KA, Guo J, Turek ME, Brogie JE, Delaney E, Luse DS, *et al.* THZ1 Reveals Roles for Cdk7 in Co-transcriptional Capping and Pausing. *Mol Cell* **2015**;59:576-87
10. Rimel JK, Taatjes DJ. The essential and multifunctional TFIIH complex. *Protein Sci* **2018**;27:1018-37
11. Branzei D, Foiani M. Regulation of DNA repair throughout the cell cycle. *Nat Rev Mol Cell Biol* **2008**;9:297-308
12. Chipumuro E, Marco E, Christensen CL, Kwiatkowski N, Zhang T, Hatheway CM, *et al.* CDK7 inhibition suppresses super-enhancer-linked oncogenic transcription in MYCN-driven cancer. *Cell* **2014**;159:1126-39
13. Kwiatkowski N, Zhang T, Rahl PB, Abraham BJ, Reddy J, Ficarro SB, *et al.* Targeting transcription regulation in cancer with a covalent CDK7 inhibitor. *Nature* **2014**;511:616-20
14. Greenall SA, Lim YC, Mitchell CB, Ensbey KS, Stringer BW, Wilding AL, *et al.* Cyclin-dependent kinase 7 is a therapeutic target in high-grade glioma. *Oncogenesis* **2017**;6:e336
15. Eliades P, Abraham BJ, Ji Z, Miller DM, Christensen CL, Kwiatkowski N, *et al.* High MITF Expression Is Associated with Super-Enhancers and Suppressed by CDK7 Inhibition in Melanoma. *J Invest Dermatol* **2018**;138:1582-90
16. Valenciaga A, Saji M, Yu L, Zhang X, Bumrah C, Yilmaz AS, *et al.* Transcriptional targeting of oncogene addiction in medullary thyroid cancer. *JCI Insight* **2018**;3:e122225
17. Wang C, Jin H, Gao D, Wang L, Evers B, Xue Z, *et al.* A CRISPR screen identifies CDK7 as a therapeutic target in hepatocellular carcinoma. *Cell Res* **2018**;28:690-2
18. Zhong L, Yang S, Jia Y, Lei K. Inhibition of cyclin-dependent kinase 7 suppresses human hepatocellular carcinoma by inducing apoptosis. *J Cell Biochem* **2018**;119:9742-51
19. Jiang YY, Lin DC, Mayakonda A, Hazawa M, Ding LW, Chien WW, *et al.* Targeting super-enhancer-associated oncogenes in oesophageal squamous cell carcinoma. *Gut* **2017**;66:1358-68

20. Yuan J, Jiang YY, Mayakonda A, Huang M, Ding LW, Lin H, *et al.* Super-Enhancers Promote Transcriptional Dysregulation in Nasopharyngeal Carcinoma. *Cancer Res* **2017**;77:6614-26
21. Christensen CL, Kwiatkowski N, Abraham BJ, Carretero J, Al-Shahrour F, Zhang T, *et al.* Targeting transcriptional addictions in small cell lung cancer with a covalent CDK7 inhibitor. *Cancer Cell* **2014**;26:909-22
22. Wang Y, Zhang T, Kwiatkowski N, Abraham BJ, Lee TI, Xie S, *et al.* CDK7-dependent transcriptional addiction in triple-negative breast cancer. *Cell* **2015**;163:174-86
23. Zhang Z, Peng H, Wang X, Yin X, Ma P, Jing Y, *et al.* Preclinical Efficacy and Molecular Mechanism of Targeting CDK7-Dependent Transcriptional Addiction in Ovarian Cancer. *Mol Cancer Ther* **2017**;16:1739-50
24. Rusan M, Li K, Li Y, Christensen CL, Abraham BJ, Kwiatkowski N, *et al.* Suppression of Adaptive Responses to Targeted Cancer Therapy by Transcriptional Repression. *Cancer Discov* **2018**;8:59-73
25. Copeland RA. Evaluation-of-Enzyme-Inhibitors-in-Drug-Discovery. John Wiley & Sons, Inc, New York, NY **2005**
26. Hafner M, Niepel M, Chung M, Sorger PK. Growth rate inhibition metrics correct for confounders in measuring sensitivity to cancer drugs. *Nat Methods* **2016**;13:521-7
27. McKeown MR, Johannessen L, Lee E, Fiore C, di Tomaso E. Antitumor synergy with SY-1425, a selective RARalpha agonist, and hypomethylating agents in retinoic acid receptor pathway activated models of acute myeloid leukemia. *Haematologica* **2018**
28. McKeown MR, Corces MR, Eaton ML, Fiore C, Lee E, Lopez JT, *et al.* Superenhancer Analysis Defines Novel Epigenomic Subtypes of Non-APL AML, Including an RARalpha Dependency Targetable by SY-1425, a Potent and Selective RARalpha Agonist. *Cancer Discov* **2017**;7:1136-53
29. Whyte WA, Orlando DA, Hnisz D, Abraham BJ, Lin CY, Kagey MH, *et al.* Master transcription factors and mediator establish super-enhancers at key cell identity genes. *Cell* **2013**;153:307-19
30. Zerbino DR, Achuthan P, Akanni W, Amode MR, Barrell D, Bhai J, *et al.* Ensembl 2018. *Nucleic Acids Res* **2018**;46:D754-D61
31. Li B, Dewey CN. RSEM: accurate transcript quantification from RNA-Seq data with or without a reference genome. *BMC Bioinformatics* **2011**;12
32. Love MI, Huber W, Anders S. Moderated estimation of fold change and dispersion for RNA-seq data with DESeq2. *Genome Biol* **2014**;15:550
33. Fabregat A, Jupe S, Matthews L, Sidiropoulos K, Gillespie M, Garapati P, *et al.* The Reactome Pathway Knowledgebase. *Nucleic Acids Res* **2018**;46:D649-D55
34. Sales G, Calura E, Romualdi C. GRAPH Interaction from pathway Topological Environment. *R package version* 1261 **2016**;10
35. Subramanian A, Tamayo P, Mootha VK, Mukherjee S, Ebert BL, Gillette MA, *et al.* Gene set enrichment analysis: A knowledge-based approach for interpreting genome-wide expression profiles. *Proc Natl Acad Sci U S A* **2005**;102:15545-50
36. Chou TC. Drug combination studies and their synergy quantification using the Chou-Talalay method. *Cancer Res* **2010**;70:440-6
37. Schwartz PA, Kuzmic P, Solowiej J, Bergqvist S, Bolanos B, Almaden C, *et al.* Covalent EGFR inhibitor analysis reveals importance of reversible interactions to potency and mechanisms of drug resistance. *Proc Natl Acad Sci U S A* **2014**;111:173-8

38. Ehmann DE, Jahic H, Ross PL, Gu RF, Hu J, Kern G, *et al.* Avibactam is a covalent, reversible, non-beta-lactam beta-lactamase inhibitor. *Proc Natl Acad Sci U S A* **2012**;109:11663-8
39. Barretina J, Caponigro G, Stransky N, Venkatesan K, Margolin AA, Kim S, *et al.* The Cancer Cell Line Encyclopedia enables predictive modelling of anticancer drug sensitivity. *Nature* **2012**;483:603-7
40. Meyers RM, Bryan JG, McFarland JM, Weir BA, Sizemore AE, Xu H, *et al.* Computational correction of copy number effect improves specificity of CRISPR-Cas9 essentiality screens in cancer cells. *Nat Genet* **2017**;49:1779-84
41. Bradner JE, Hnisz D, Young RA. Transcriptional Addiction in Cancer. *Cell* **2017**;168:629-43
42. VENCLEXTA® (venetoclax tablets)[package insert]. North Chicago (IL): AbbVie Inc. **2016**
43. Thomas LW, Lam C, Edwards SW. Mcl-1; the molecular regulation of protein function. *FEBS Lett* **2010**;584:2981-9

Figure legends:

Fig.1. Features of SY-1365 and related molecules. **(A)** Characteristics of key molecules from the progression of THZ1 to SY-1365. **(B)** Model of SY-1365 binding the active site of CDK7. **(C)** SY-1365 potency and selectivity against other CDK enzymes at both K_M and 2 mM [ATP]. The best fit IC_{50} values are listed in Supplementary Table S5 for SY-1365 and related compounds described for a subset of CDK enzymes.

Fig. 2. CDK7 target engagement following treatment with inhibitors, and changes in CDK7 downstream targets upon SY-1365 treatment. **(A)** HL60 cells were treated with indicated compounds for 1hr and free (reacted with biotinylated CDK7-inhibitor) and total CDK7 were visualized by immunoblotting with anti-CDK7 antibody. The quantification is shown in Supplementary Table S8A. **(B)** HL60 cells were treated for 1hr with eight concentrations of THZ1, SY-314, SY-351 and SY-1365. CDK7 target engagement was determined by the MSD plate-based method as described in methods. EC_{50} and EC_{90} target occupancies for each compound are listed in Supplementary Table S7. **(C)** THP1 cells were treated with indicated dosage of SY-1365, protein samples were collected at 6, 24 and 48h post treatment. Phospho-CDK2 T160, RNAPII Ser2,5 and 7 phosphorylation level and total RNAPII protein level were measured by immunoblotting. CDK7 target engagement was measured in the samples by immunoblotting. Tubulin was used as loading control. The quantification is shown in Supplementary Table S8B. All immunoblot data are quantified by ImageJ. Experiments were performed independently at least three times.

Fig. 3. Distribution of growth parameters in response to SY-1365 for 376 human cancer cell lines across 21 indications. Cells were incubated with compound for 72 h or at least two doubling times if they were slow growing. Drug sensitivity metrics include **(A)** GR_0, lowest concentration at which cell death is induced. **(B)** GR_{max}, magnitude of cell death (0 means no net change in cell number; -1 means no detectable cells). **(C)** IC_{50}, concentration of SY-1365 at which cells undergo 50% reduction in cell proliferation. Boxplot statistics are as follows: the box boundaries represent the inter-quartile range with the midline as the median of the data, whiskers extend to the most extreme data point that is less than or equal to 1.5 times the interquartile range from the boundary of the box.

Fig. 4. SY-1365 treatment induced apoptosis in AML and TNBC cell lines but not in immortalized normal cell lines. **(A)** THP1, ML-2, MDA-MB-468, HCC70, RPE-hTERT and BJ-hTERT cells were treated with SY-1365 for 48h and percentage of cells undergoing apoptosis determined by flow cytometry following annexin V-FITC and Propidium iodide (PI) staining. Data shows mean population from three independent experiments with standard deviation as error bars. **(B)** THP1 (AML), HCC70 (TNBC) and RPE-hTERT (immortalized normal) cells were treated with SY-1365 for 6, 24 and 48 hours and dose dependent changes in PARP cleavage were analyzed by Western blot. Tubulin was used as loading control. This experiment was part of the same western blot as in Fig. 4B and Supplementary Fig. S4, and the tubulin loading control blots are the same in the figures for each cell line. Experiments were performed at least three times.

Fig. 5. Relationship of response to SY-1365 with BCL-XL expression and MCL1 essentiality. **(A)** SY-1365 Growth-Response (GR) Curves for 386 human cancer cell lines colored by their assignment to “low” (blue) and “high” (red) sensitivity groups. **(B)** Distribution of expression of the BCL2L1 gene, measured by either microarray (n=303) or RNA-Seq (n=294), within groups of cell lines classified as having “low” or “high” sensitivity to SY-1365. Boxplot statistics are as described in Fig.3. **(C)** THP1 (AML), HCC70 (TNBC) and RPE-hTERT (immortalized normal) cells were treated with SY-1365 for 6, 24 and 48 hours and MCL1 protein level was analyzed by immunoblotting with tubulin used as a loading control. This experiment was part of the same western blot as in Fig.4B and Supplementary Fig.S4. and the tubulin loading control blots are the same in the two figures. The immunoblot data was quantified by ImageJ. The quantification is shown in Supplementary Table S10. Experiments were performed at least three times. **(D)** Distribution of MCL1 essentiality within groups of cell lines classified as having “low” or “high” sensitivity to SY-1365 (n=109). Boxplot statistics are as described in Fig. 3.

Fig. 6. Transcriptional changes induced by SY-1365. **(A)** Principal component analysis of THP-1 cell lines treated with various transcriptional drugs for 2 and 6 hours. **(B)** Examples of genes significantly down-regulated upon SY-1365 treatment (n=3) belonging to REACTOME pathways enriched for down regulated genes associated with cell cycle, homologous damage repair and mismatch repair, or oncogenes with super-enhancers (SE) that rank among the top 50 strongest SEs in THP1. Housekeeping genes with high basal expression relatively unchanged upon SY-1365 treatment are shown as reference. **(C)** p-value of enrichment of genes down regulated by SY-1365 in

THP-1 cells within 1208 REACTOME pathways are plotted against the p-value of enrichment of genes down regulated within the same pathways in CDK7 analog sensitive HCT116 cells compared to wildtype HCT116 cells (both treated with 10uM 3NM-PP1 for 24 hours). Pathways with p-value < 0.001 for both datasets as well as a few additional DNA damage pathways of interest are numbered in increasing order of average p-value across both datasets. Pathway names corresponding to the numbers are shown below the plot.

Fig. 7. Anti-tumor effect of SY-1365 in AML and ovarian cancer models *in vivo* as single agent and in combination with venetoclax. SY-1365 was dosed in **(A)** Kasumi-1 AML cell line derived, **(B)** ML-2 AML cell line derived, **(C)** OVCAR3 ovarian cancer cell line derived (CDX) and **(D)** OV15398 high grade serous ovarian cancer patient derived xenograft models (PDX). **(E)** SY-1365 and venetoclax were dosed in the KG-1 xenograft model. Tumor volumes were measured twice weekly in two dimensions by caliper. Treatment details for each group are listed in Supplementary Table S4.

A

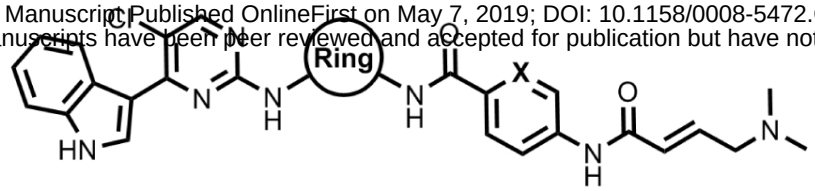

Compound	Ring	X	k_{inact} (h^{-1})	K_I (nM)	k_{inact} / K_I ($\mu M^{-1}s^{-1}$)	Cellular antiproliferation EC_{50} (nM)	Cellular CDK7 target occupancy EC_{50} (nM)	CI (mL/min/kg)
THZ-1		CH	2.78	255	0.003	38	101	129
SY-314		CH	4.75	105	0.013	13	48	17
SY-351		N	11.3	62.5	0.050	3	4	29
SY-1365		N	8.21	17.4	0.131	8	13	5.6

B

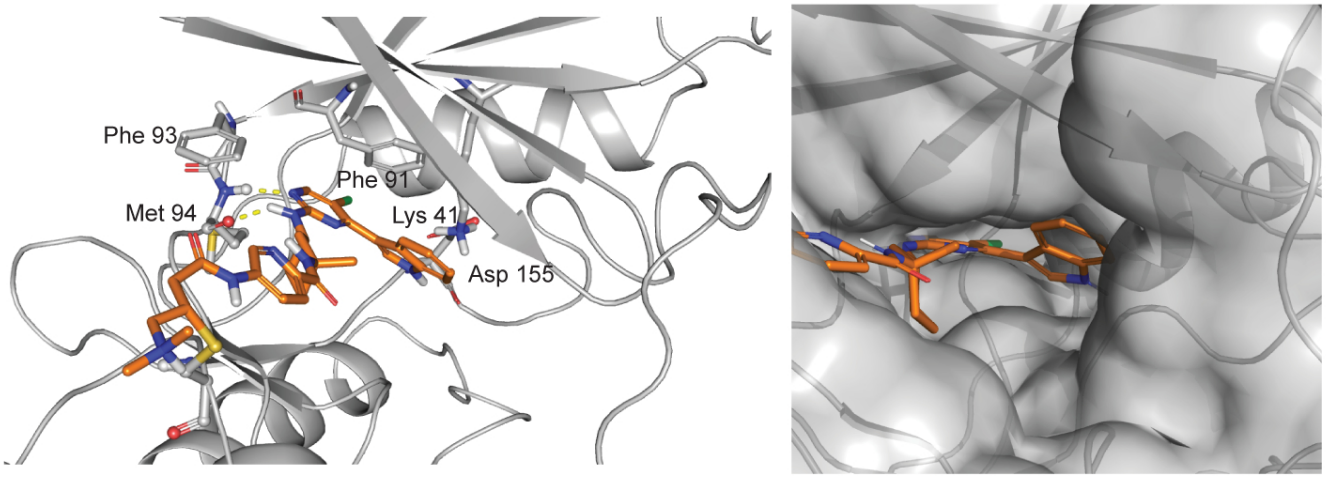

C

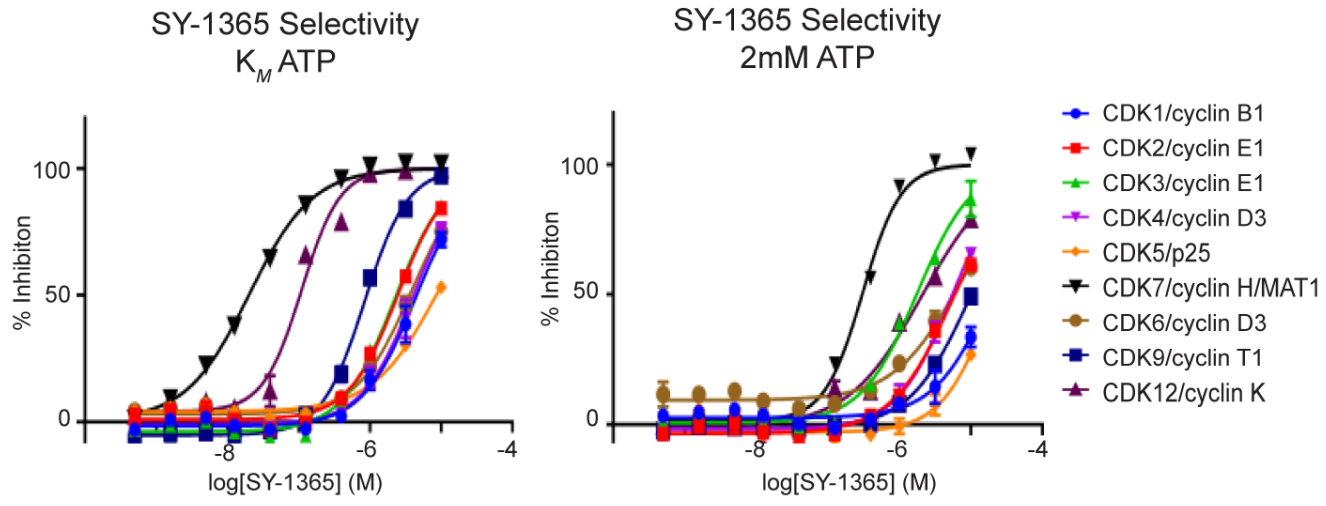

Figure 1

Author Manuscript Published OnlineFirst on May 7, 2019; DOI: 10.1158/0008-5472.CAN-19-0119
Author manuscripts have been peer reviewed and accepted for publication but have not yet been edited.

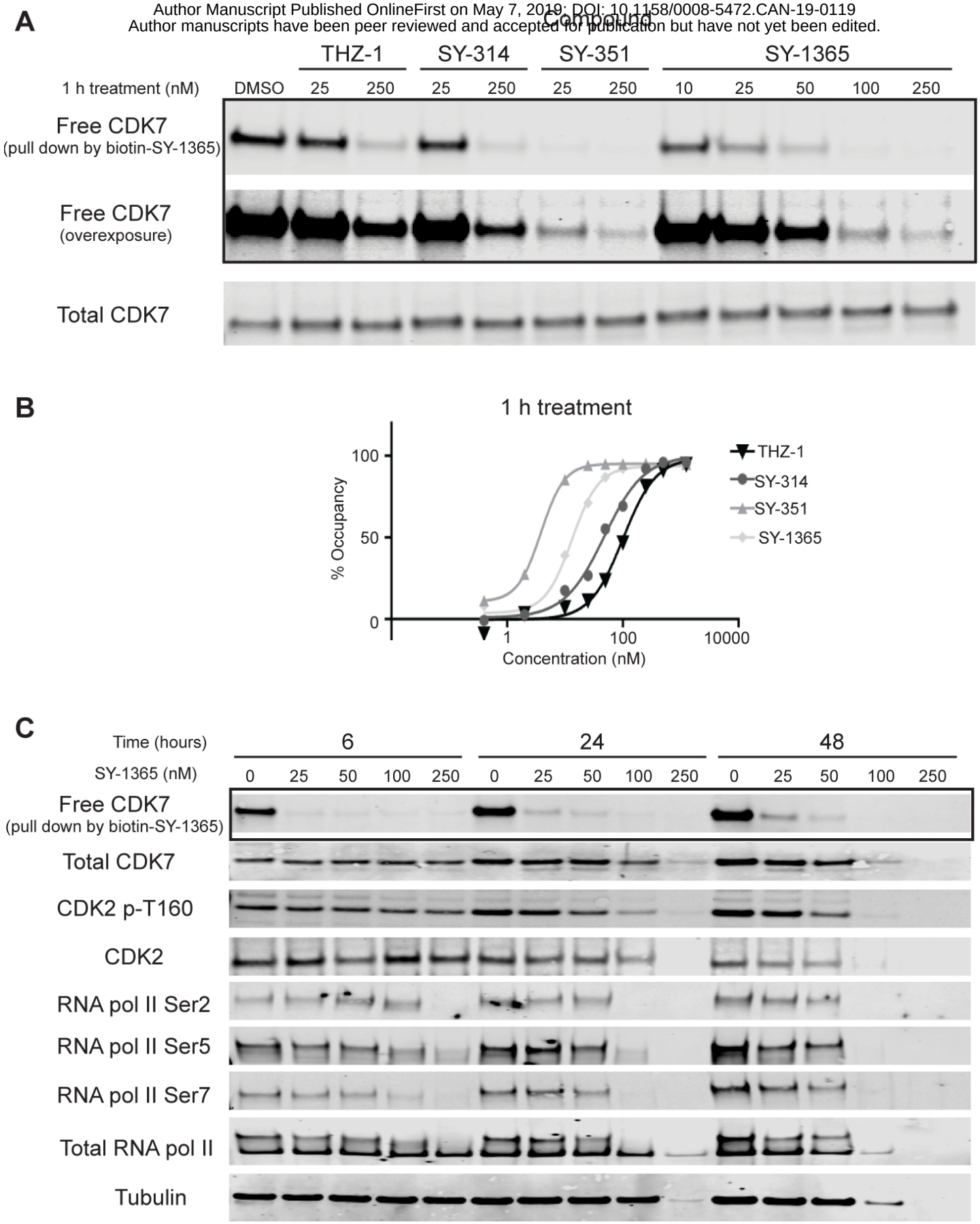

Figure 2

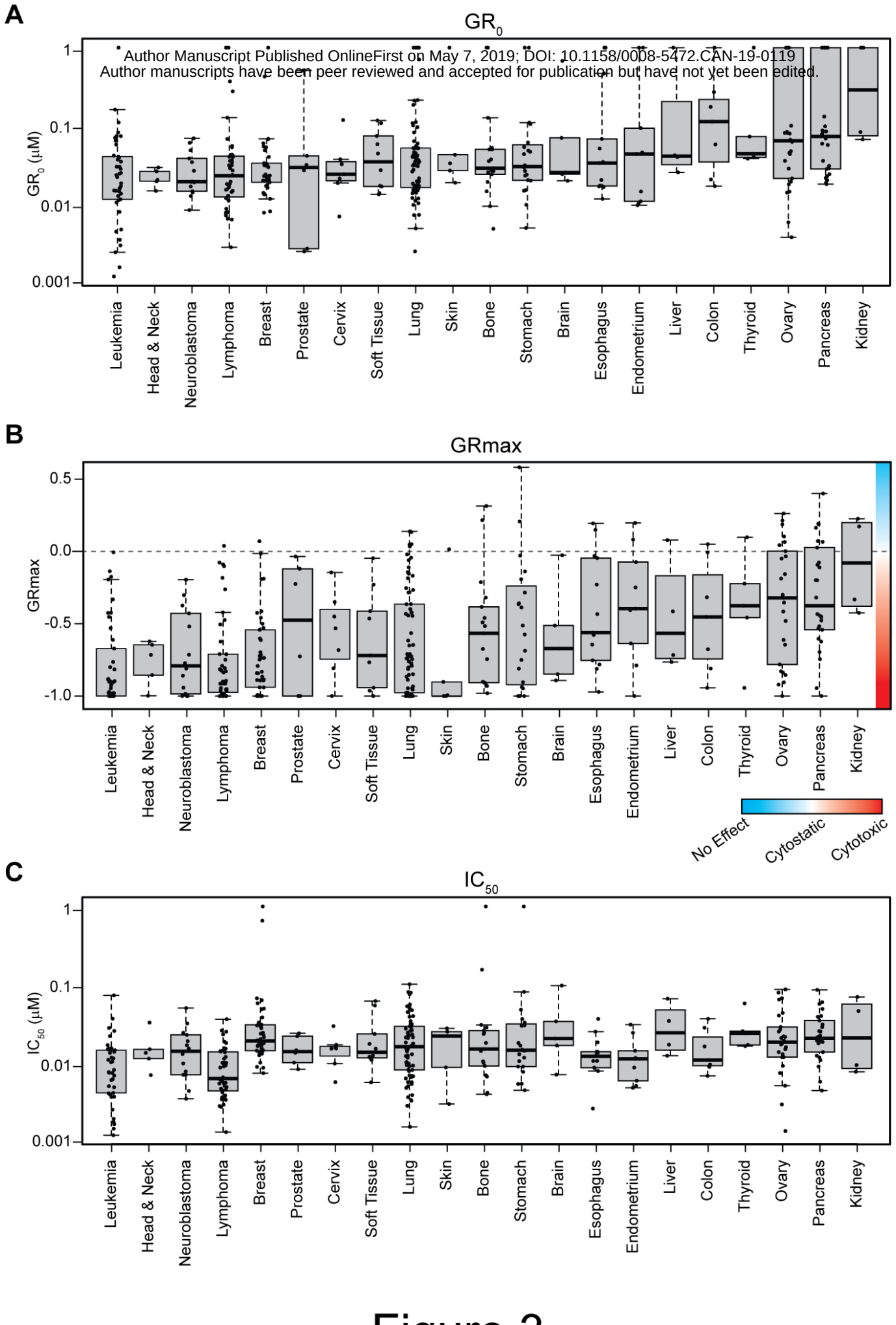

Figure 3

Author Manuscript Published OnlineFirst on May 7, 2019; DOI: 10.1158/0008-5472.CAN-19-0119
Author manuscripts have been peer reviewed and accepted for publication but have not yet been edited.

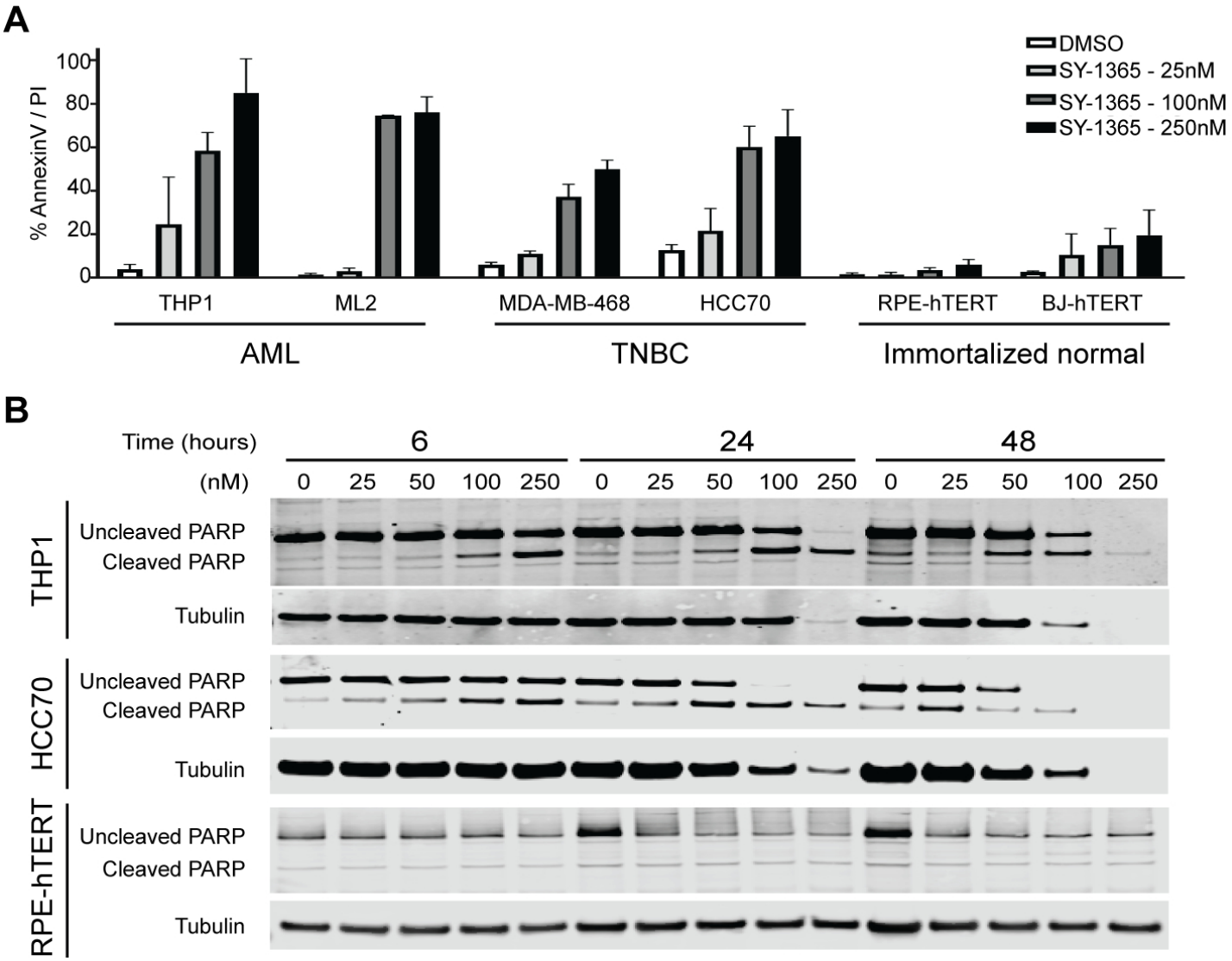

Figure 4

Author Manuscript Published OnlineFirst on May 7, 2019; DOI: 10.1158/0008-5472.CAN-19-0119
Author manuscripts have been peer reviewed and accepted for publication but have not yet been edited.

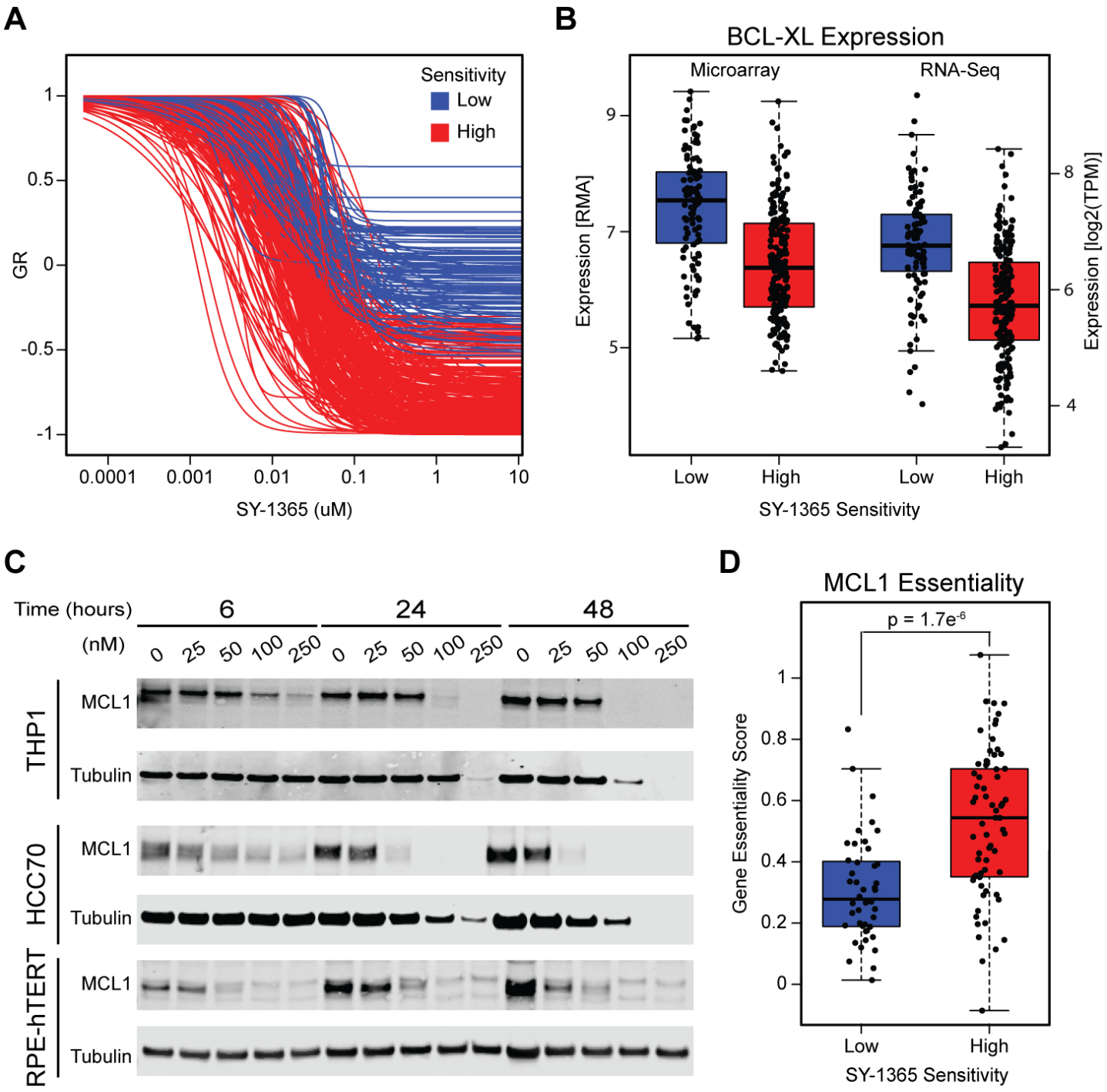

Figure 5

Author Manuscript Published OnlineFirst on May 7, 2019; DOI: 10.1158/0008-5472.CAN-19-0119
Author manuscripts have been peer reviewed and accepted for publication but have not yet been edited.

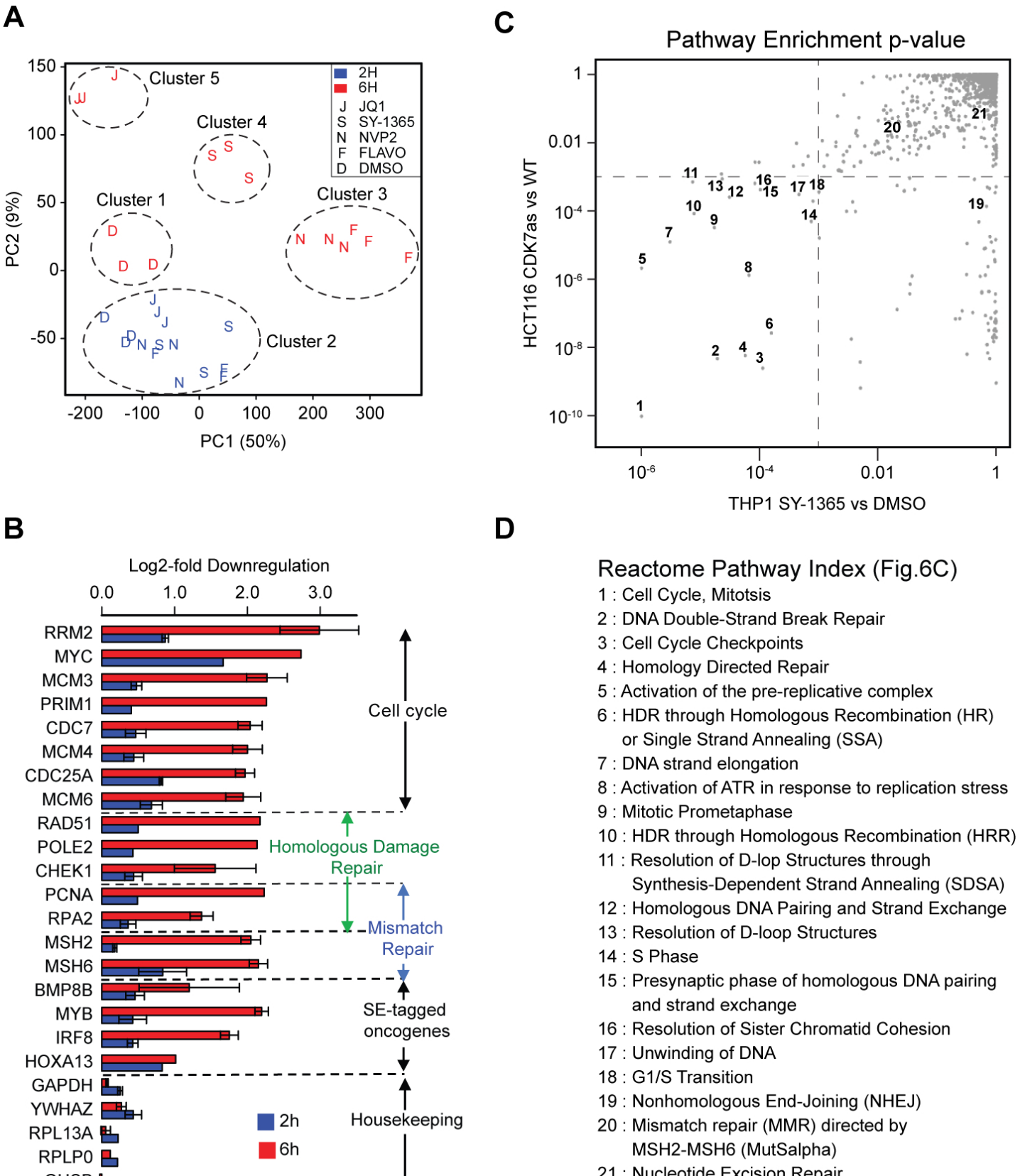

Figure 6

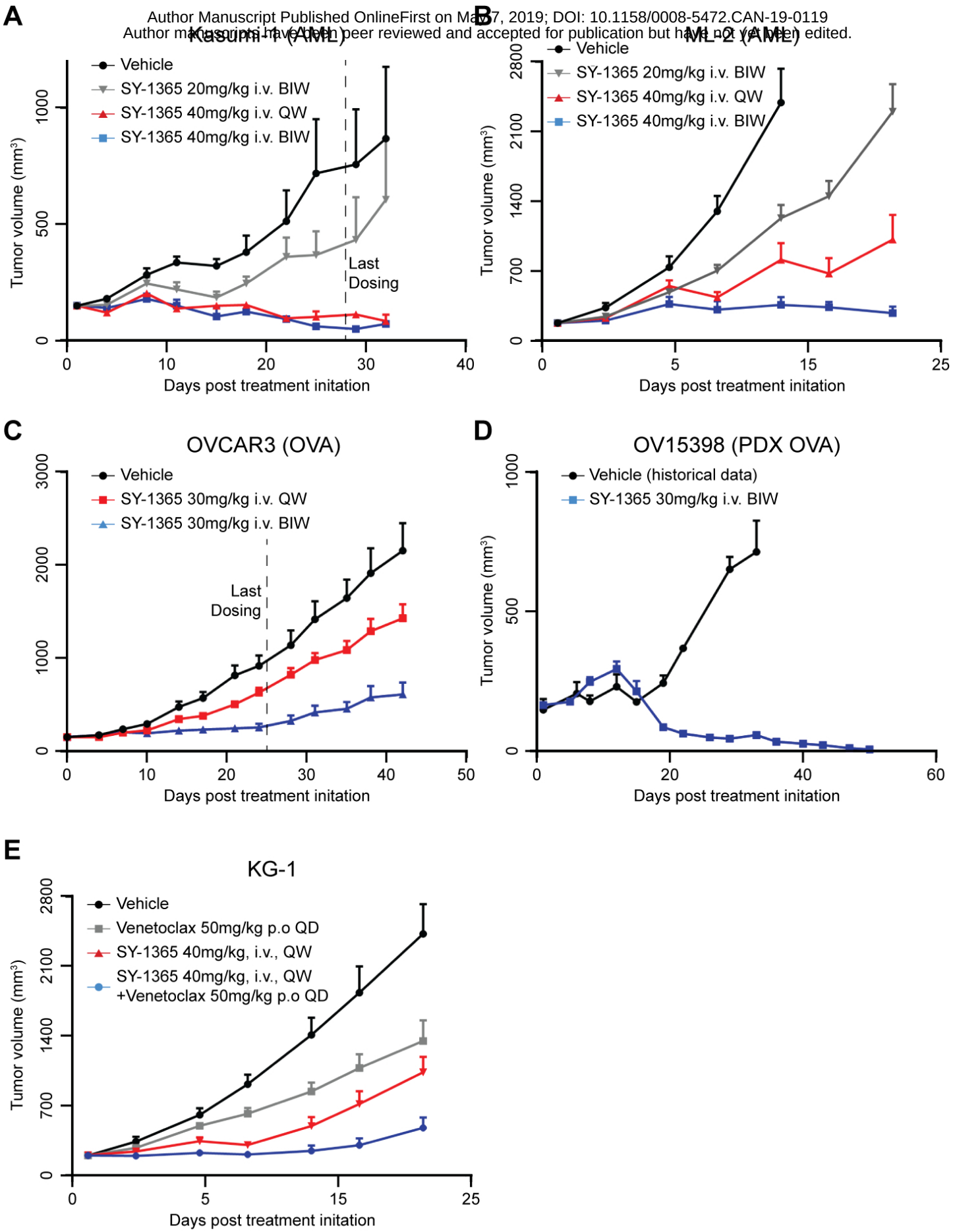

Figure 7

Cancer Research
The Journal of Cancer Research (1916–1930) | The American Journal of Cancer (1931–1940)

AACR American Association for Cancer Research

Discovery and characterization of SY-1365, a selective, covalent inhibitor of CDK7

Shanhu Hu, Jason J Marineau, Nisha Rajagopal, et al.

Cancer Res Published OnlineFirst May 7, 2019.